GMR
The Original

ULTRASOUND-ASSISTED SYNTHESIS, SPECTROSCOPIC CHARACTERIZATION, AND MOLECULAR DOCKING OF NOVEL BENZO[G]PTERIN-BASED HETEROCYCLIC DERIVATIVES TOWARD HUMAN DIHYDROFOLATE REDUCTASE

Karm A. Khalaf[1], Adnan O. Omar[2]

[1*,2]Department of Chemistry, College of Science, University of Mosul, Mosul, Iraq, karm.21scp47@student.uomosul.edu.iq and adnana.hasska94@uomosul.edu.iq

ABSTRACT:
A series of Benzo[g]pterin-based heterocyclic derivatives was prepared through an ultrasound-assisted synthetic strategy. Five Schiff-base intermediates generated from an amino-Benzo[g]pterin scaffold and substituted aromatic aldehydes were used as key precursors for subsequent ring-forming reactions. Three families of cyclized products were obtained: azetidin-2-one (beta-lactam) derivatives L1–L5, imidazole derivatives G1–G5, and tetrazole derivatives T1–T5. The reported reactions were generally completed after 40 min of ultrasonic irradiation, and the isolated yields of the listed Schiff bases and cyclized compounds ranged from 60 to 85%. Structural assignments were supported by melting-point data, FT-IR spectroscopy, 1H NMR, and 13C NMR spectroscopy. Schiff-base formation was indicated by the appearance of azomethine resonances, whereas cyclization was supported by the loss or transformation of the azomethine environment and the appearance of new saturated-ring carbon/proton signals together with diagnostic carbonyl or heterocyclic features. Computational evaluation was performed against human dihydrofolate reductase (hDHFR; PDB ID 1U72) using CB-Dock2 and post-docking visualization with BIOVIA Discovery Studio Visualizer. The three best reported docking scores were -11.2, -11.1, and -10.8 kcal mol-1, corresponding to a brominated beta-lactam derivative (L2), a methylenedioxy-substituted imidazole derivative (G4), and a brominated tetrazole derivative (T2), respectively. These molecular docking results suggest that compounds L2, G4, and T2 possess promising binding affinity towards hDHFR, making them potential candidates for further biological evaluation.

KEYWORDS: Benzo[g]pterin; ultrasound-assisted synthesis; Schiff base; azetidin-2-one; beta-lactam; imidazole; tetrazole; molecular docking; human DHFR

INTRODUCTION

Heterocyclic compounds represent an essential pillar of medicinal chemistry owing to their diverse structural architectures and versatility in interacting with biological macromolecules [1]. Among nitrogen-rich heterocycles, pteridine derivatives and their fused analogs constitute a crucial class of bioactive pharmacophores [2]. The core pterin structure serves as a fundamental building block in naturally occurring biomolecules, most notably folic acid (Vitamin B9) and tetrahydrobiopterin (BH4), which act as essential cofactors in nucleotide biosynthesis and critical metabolic pathways [3]. Consequently, structural modifications of the fused Benzo[g]pterin scaffold offer an attractive platform for designing antimetabolites capable of targeted molecular recognition [4].
Molecular hybridization has emerged as a powerful synthetic paradigm for fusing distinct heterocyclic motifs into a single molecular framework to enhance target affinity and optimize physicochemical properties [5]. In this regard, integrating \beta-lactam, imidazole, and tetrazole rings into the Benzo[g]pterin core is particularly promising. The four-membered β-lactam ring introduces structural strain and hydrogen-bonding capabilities, whereas the nitrogen-dense imidazole and tetrazole heterocycles modulate molecular polarity and intermolecular binding networks [6]. Schiff bases, characterized by the azomethine linker (-CH=N-), function as pivotal synthetic intermediates for constructing these cyclizedarchitectures[7].
Green chemistry protocols, such as ultrasound-assisted organic synthesis, significantly facilitate these transformations by improving mass transfer and accelerating reaction kinetics through acoustic cavitation [8]. In the present study, a series of novel Benzo[g]pterin-based Schiff bases was synthesized and efficiently converted into β-lactam, imidazole, and tetrazole derivatives under ultrasonic irradiation within short reaction times (40 min) to afford good yields. All synthesized compounds were structurally elucidated using melting point determination, FT-IR, 1H-NMR, and 13C-NMR spectroscopy. Furthermore, computational molecular docking was carried out against human dihydrofolate reductase (hDHFR; PDB ID: 1U72) a central therapeutic target in cellular proliferation to evaluate their ligand-protein binding interactions and identify promising candidate structures for future biological evaluation.

2. MATERIALS AND METHODS

2.1.MaterialsandInstrumentation

All chemicals, solvents, and reagents were obtained from commercial suppliers and used as received without further purification. Absolute ethanol was used as the primary reaction solvent, glacial acetic acid as the catalyst for Schiff-base formation, chloroacetyl chloride and sodium bicarbonate (NaHCO3) for azetidin-2-one derivatives, glycine for imidazole derivatives, and sodium azide (NaN3) for tetrazole derivatives. Reaction progress and structural characterizations were accomplished using standard analytical techniques. Melting points were determined using an open capillary melting point apparatus. FT-IR spectra were recorded on a Bruker FT-IR spectrometer in the wavenumber range of 4000-400 cm-1 using KBr pellets. Nuclear magnetic resonance spectra (1H-NMR at 400.13 MHz and 13C-NMR at 100.62 MHz) were acquired on a Bruker AVANCE NEO 400 MHz spectrometer using deuterated dimethyl sulfoxide (DMSO_d6) as the solvent. Chemical shifts (δ) are expressed in parts per million (ppm) relative to tetramethylsilane (TMS) as an internal reference. Peak multiplicities are reported using standard abbreviations: s (singlet), d (doublet), t (triplet), m (multiplet), and br (broad).

2.2 General procedure for Schiff-base intermediates

An equimolar mixture of amino-Benzo[g]pterin (0.005 mol) and the designated aromatic aldehyde (0.005 mol) was dissolved in absolute ethanol (20 mL), followed by the addition of glacial acetic acid (5 drops) as a catalyst. The reaction mixture was subjected to ultrasonic irradiation at 60 C for 40 min. Upon reaction completion, cold water was added to induce precipitation [9-10]. The solid precipitate was collected by filtration, washed with cold water, dried, and purified by recrystallization using ethanol as the solvent to yield the pure Schiff bases (B, Br, V, P, and S) as shown in Scheme 1.

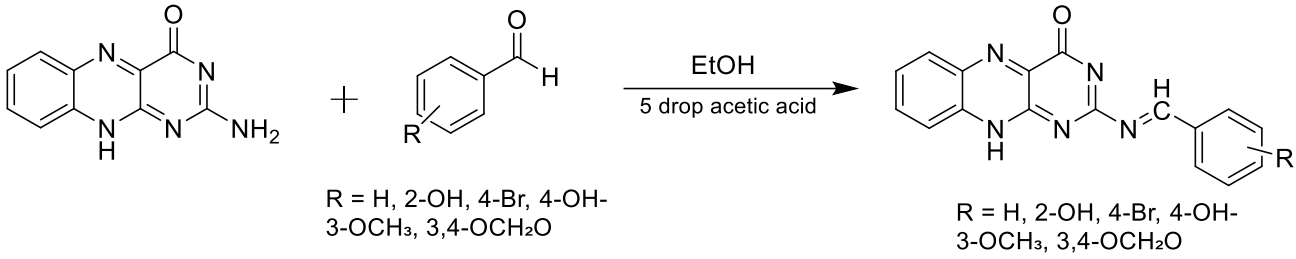

Scheme 1. Synthetic route for the preparation of Schiff-base intermediates (B, Br, V, P, S).

2.3. General procedure for the synthesis of azetidin-2-one (β-lactam) derivatives (L1–L5)

A mixture of the appropriate Schiff base (0.005 mol) and chloroacetyl chloride (0.005mol, 1 equiv) in absolute ethanol (20 mL) was prepared in the presence of sodium bicarbonate (NaHCO3, 0.005 mol) as a base. The reaction mixture was subjected to ultrasonic irradiation at 60C for 40min. After completion, cold distilled water was added gradually to the mixture with stirring to ensure complete precipitation [11-12]. The solid product was collected by filtration, washed thoroughly with cold water, dried, and purified by recrystallization using ethanol as the solvent to yield the pure β-lactam derivatives (L1–L5 as shown in Scheme 2.

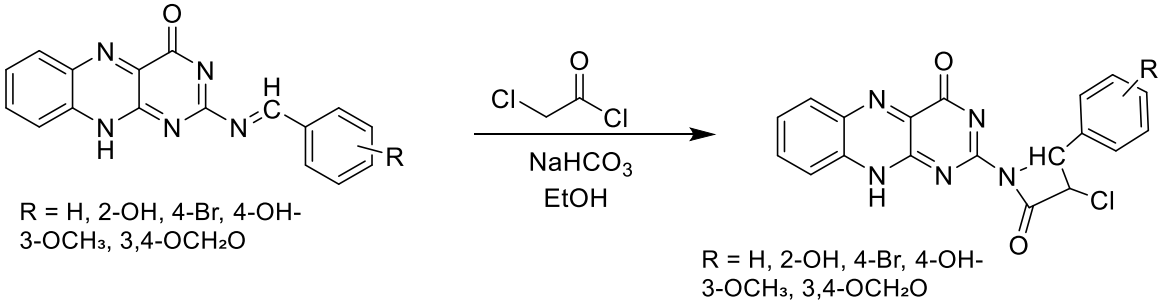

Scheme 2. Synthesis of azetidin-2-one (β-lactam) derivatives (L1-L5).

2.4. General procedure for the synthesis of imidazole derivatives (G1–G5)

An equimolar mixture of the appropriate Schiff base (0.005 mol) and glycine (0.005 mol) was dissolved in absolute ethanol (20 mL). The reaction mixture was subjected to ultrasonic irradiation at 40C for 40 min to promote cyclocondensation with the loss of water. Upon completion, the reaction mixture was allowed to cool to room temperature, and cold water was added to complete precipitation [13-14]. The solid precipitate was collected by filtration, washed with cold water, dried, and purified by recrystallization using ethanol as the solvent to yield the pure imidazole derivatives (G1–G5) as shown in Scheme 3.

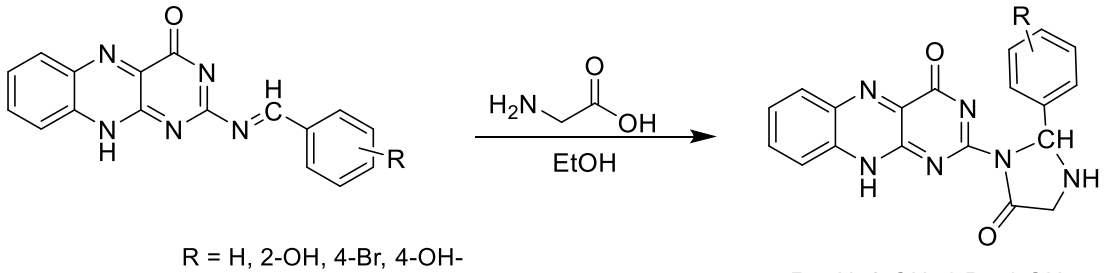

Scheme 3. Synthesis of imidazole derivatives (G1-G5).

2.5. General procedure for the synthesis of tetrazole derivatives (T1–T5)

An equimolar mixture of the appropriate Schiff base (0.005 mol) and sodium azide (NaN3, 0.005 mol) was dissolved in absolute ethanol (20 mL). The reaction mixture was subjected to ultrasonic irradiation at 60C for 40 min. Upon completion, cold distilled water was added gradually to the mixture with continuous stirring to ensure complete precipitation [15-16]. The solid product was collected by filtration, washed thoroughly with cold water, dried, and purified by recrystallization using ethanol as the solvent to yield the pure tetrazole derivatives (T1–T5) as shown in

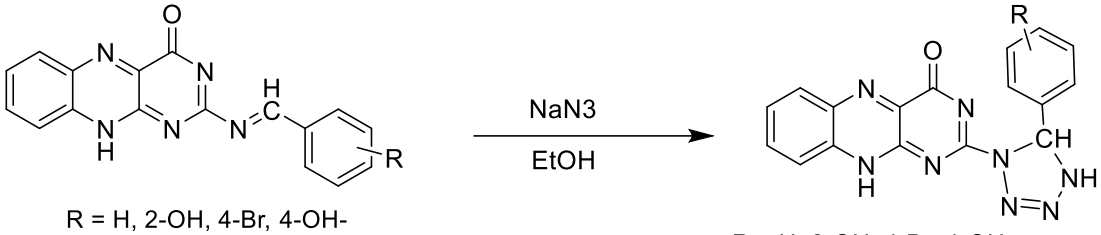

Scheme 4.

Scheme 4. Synthesis of tetrazole derivatives (T1-T5).

2.6 Molecular docking protocol

Human dihydrofolate reductase was selected as the receptor. The crystallographic structure PDB 1U72 was obtained from the Protein Data Bank [17]. This entry is wild-type Homo sapiens DHFR in a ternary complex with methotrexate and NADPH, determined by X-ray diffraction at 1.90 Å resolution [18]. In the supplied workflow, solvent molecules and the co-crystallized reference inhibitor were removed to prepare the receptor for docking. The reported docking center was X = 20.37, Y = 5.60, and Z = −2.25.

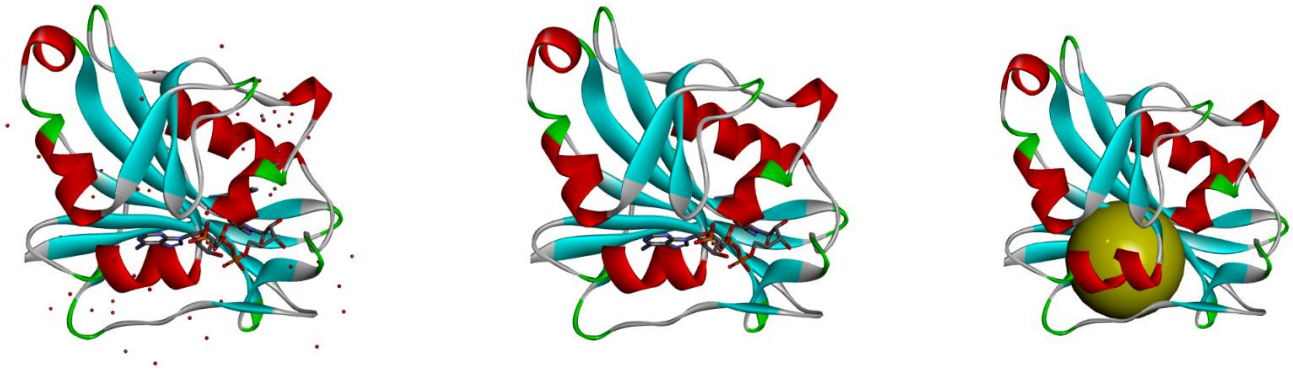

A B C

Figure 1. (A) Enzyme with ligand and solvent; (B) cleaned enzyme without ligand and solvent; (C) enzyme with the identified active site.

Table 1. Molecular docking scores and binding energies of the top-performing compounds against human DHFR (PDB 1U72).

Compound	Structural feature	Docking score (kcal mol−1)	Comment
L2	Brominated β-lactam	−11.2	Highest reported docking score
G4	Methylenedioxy imidazole	−11.1	Second-highest reported score
T2	Brominated tetrazole	−10.8	Third-highest reported score

Molecular docking results revealed that compounds L2, G4, and T2 exhibited the most favorable binding energies among all the investigated compounds, indicating their stronger predicted binding affinities toward the active site of the enzyme. L2 showed the best binding energy of −11.2 kcal/mol, ranking first among the three compounds, followed by G4 with a binding energy of −11.1 kcal/mol. In contrast, T2 exhibited a binding energy of −10.8 kcal/mol, which was

the least negative value among the three selected compounds, while still remaining among the most favorable results compared with the other investigated compounds [19]. Accordingly, the predicted binding affinity followed the order L2 > G4 > T2. Furthermore, the binding modes and interactions of these compounds with amino acid residues within the binding site were analyzed using Discovery Studio, as illustrated by the two-dimensional (2D) and three-dimensional (3D) representations in Figure (2) and (3), which demonstrate the orientation of the compounds within the binding pocket and the interactions contributing to the stability of the protein–ligand complexes [20].

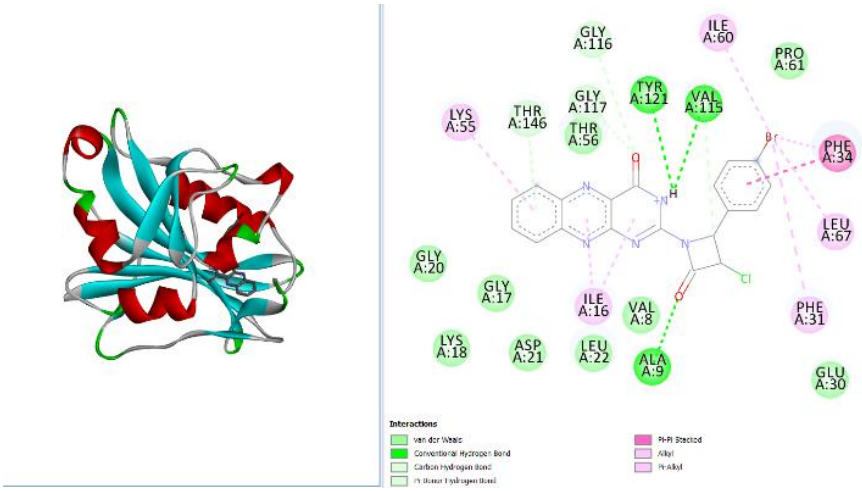

Figure 2. 3D and 2D molecular docking interaction profiles of compound L2 within the active site of human DHFR (PDB 1U72)

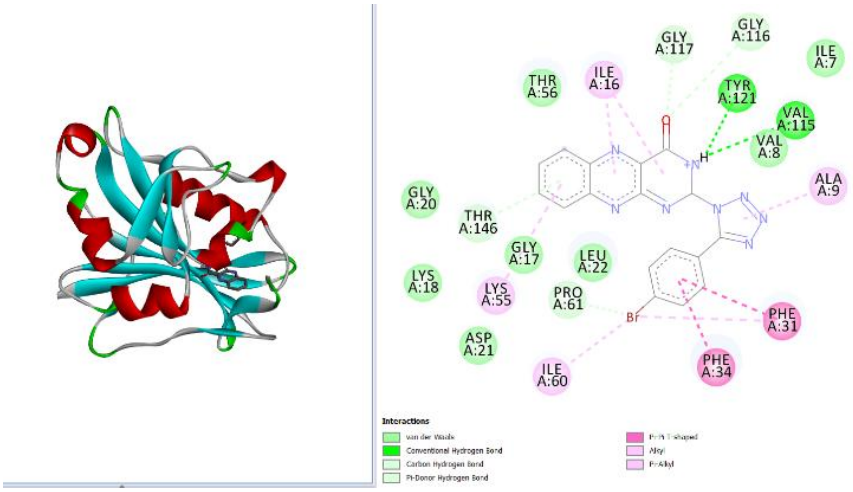

Figure 3. 3D and 2D molecular docking interaction profiles of compound G4 within the active site of human DHFR (PDB 1U72).

3. RESULTS AND DISCUSSION

3.1 Synthesis and physical properties

The synthetic sequence produced five Schiff-base intermediates followed by three cyclized series. The reported yields were moderate to good (60–85%). The highest isolated yield in the compiled dataset was 85%, observed for the brominated β-lactam L2 and the brominated imidazole G2. Physical-property data are summarized in Table 2.

Code	Structure	M.P(°C)	Yield (%)	Color	Molecular formula	M.W.
B	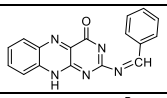	133	60	Red	C17H11N5O	301.31
Br	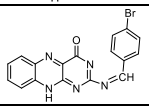	138	80	Orange	C17H10BrN5O	380.21
V	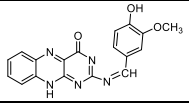	208	70	Red	C18H13N5O3	347.33

Code	Structure	M.P(°C)	Yield (%)	Color	Molecular formula	M.W.
P	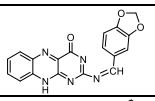	123	60	Black	C18H11N5O3	345.32
S	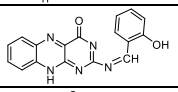	211	65	Yellow	C17H11N5O2	317.31
L1	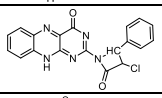	212	60	Brown	C19H12ClN5O2	377.79
L2	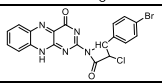	230	85	Orange	C19H11BrClN5O2	456.68
L3	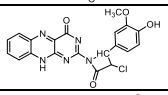	226	80	Yellow	C20H14ClN5O4	423.81
L4	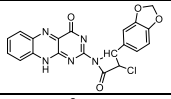	198	65	Brown	C20H12ClN5O4	421.80
L5	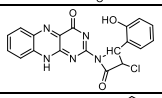	228	60	Red	C19H12ClN5O3	393.79
G1	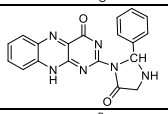	267	80	Yellow	C19H14N6O2	358.36
G2	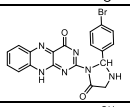	142	85	Orange	C19H13BrN6O2	437.26
G3	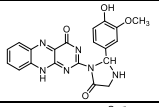	160	70	Yellow	C20H16N6O4	404.39
G4	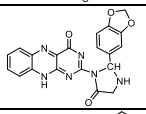	122	80	Brown	C20H14N6O4	402.37
G5	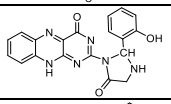	223	75	Yellow	C19H14N6O3	374.36
T1	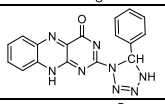	232	75	Orange	C17H12N8O	344.34
T2	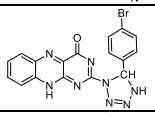	218	65	Black	C17H11BrN8O	423.23
T3	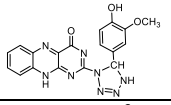	245	70	Brown	C18H14N8O3	390.36
T4	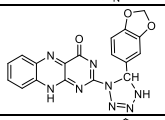	220	60	Brown	C18H12N8O3	388.35
T5	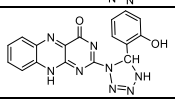	230	70	Yellow	C17H12N8O2	360.34

3.2 Spectroscopic characterization of Schiff-base intermediates

The most diagnostic feature of Schiff-base formation is the appearance of an azomethine N=CH environment. In the reported 1H NMR spectra, this proton appeared between approximately δ 8.38 and 8.51 ppm for the substituted derivatives, while the unsubstituted phenyl derivative was reported as a multiplet contribution near δ 7.96–7.88 ppm. NH signals were observed close to δ 9.77–10.26 ppm. Substituent-specific resonances, such as OCH3 and O–CH2–O, were also present. The 13C NMR data included a carbonyl resonance around δ 166–170 ppm and multiple heteroaromatic C=N (Sp2) carbon signals. The reported data are summarized in Table 3.

Compound	1H NMR, DMSO-d6, δ (ppm)	13C NMR, DMSO-d6, δ (ppm)	FT-IR, KBr (cm−1)
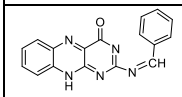	10.025 (s, 1H, NH); 7.96–7.88 (m, 1H, N=CH); 7.88–7.60 (m, 4H, fused Ar–H); 7.60–7.29 (m, 5H, phenyl Ar–H)	169.16 (C=O); 162.34, 162.14, 158.88, 150.33, 149.84 (heterocyclic C); 136.14, 134.04, 133.97, 133.84, 133.50, 133.33, 132.20, 131.34, 129.50, 127.77, 125.57	1730 (C=O); 1524, 1603, 1652 (C=N region); 1503 (C=C); 3054 (NH); 2845 (C–H)
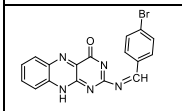	9.977 (s, 1H, NH); 8.513 (s, 1H, N=CH); 7.993–7.833, 7.813–7.583, 7.564–7.344 (Ar–H)	166.44 (C=O); 155.03 (C=N); 139.02, 138.52, 137.51, 136.04, 132.79, 132.50, 132.20, 131.84, 131.34, 129.51, 128.97, 128.73, 128.67, 122.90, 122.18	1720; 1566, 1592, 1678; 1505; 3087 (NH); 2833 (C–H)
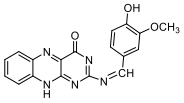	10.284 (s, 1H, OH); 9.773 (s, 1H, NH); 8.508 (s, 1H, N=CH); 7.985–7.873, 7.602–7.229, 6.973–6.811 (Ar–H); 3.843 (s, 3H, OCH3)	169.53 (C=O); 163.48 (Ar–C–OH); 153.47, 148.61 (C=N); 142.96, 142.68, 138.83, 134.55, 129.15, 128.98, 126.55, 119.98, 119.55, 117.15, 115.83, 115.73, 111.10; 56.03 (OCH3)	1730; 1587, 1588, 1656; 1507; 3361 (OH); 3178 (NH); 2846 (C–H)
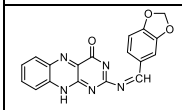	9.810 (s, 1H, NH); 8.383 (s, 1H, N=CH); 7.561–7.538, 7.329–7.136 (Ar–H); 6.178–6.126 (s, 2H, O–CH2–O)	169.48 (C=O); 158.89, 158.84, 153.24, 148.83; aromatic/heterocyclic carbons 138.93–106.73; 102.81 (O–CH2–O)	1726; 1599, 1622, 1668; 1523; 3103 (NH); 2850 (C–H)
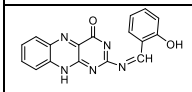	10.724 (s, 1H, OH); 10.264 (s, 1H, NH); 8.507 (s, 1H, N=CH); 8.297–7.880, 7.608–7.229 (Ar–H)	169.53 (C=O); 163.48 (Ar–C–OH); 153.47, 148.61 (C=N); remaining aromatic/heterocyclic carbons as reported	1730; 1522, 1608, 1651; 1504; 3176 (OH); 3089 (NH); 2890 (C–H)

3.3 Spectroscopic characterization of β-lactam derivatives L1–L5

Cyclization to the azetidin-2-one series was supported by the appearance of new saturated ring proton signals assigned to CH–Ar and CH–Cl, generally in the δ 4.0–4.6 ppm region, and corresponding 13C NMR resonances near δ 52–62 ppm. The source data also report two carbonyl environments attributable to the Benzo[g]pterin carbonyl and the β-lactam carbonyl. The presence of a C–Cl absorption in the approximately 582–609 cm−1 region was reported for this series The reported data are summarized in Table 4.

Code	1H NMR	13C NMR	FT-IR
L1	10.0 (s, 1H, NH); 8.3–7.8 and 7.7–7.2 (Ar–H); 4.5 (1H, CH–Ph); 4.1 (1H, CH–Cl)	168.2, 165.3 (C=O); 156.0, 153.2; 140.0; aromatic C 133.5–123.0; 62.3 (CH–Cl); 55.5 (CH–Ph)	1731; 1512, 1567, 1593; 1675; 3102 (NH); 609 (C–Cl)
L2	10.0 (s, 1H, NH); 8.3–7.8 (m, 4H); 7.8–7.4 (m, 4H); 4.4 (1H, CH); 4.0 (1H, CH–Cl)	166.72, 164.12 (C=O); 155.02, 152.93; aromatic/heterocyclic C 132.85–122.04; 62.33 (CH–Cl); 56.43 (CH)	1727; 1504, 1525, 1605; 1659; 3100 (NH); 582 (C–Cl)
L3	10.723 (s, 1H, OH); 9.884 (s, 1H, NH); 8.488–8.484 (1H, CH); 8.261–7.865, 7.593–7.297 (Ar–H); 4.621–4.109 (1H, CH–Cl); 3.817–3.702 (s, 3H, OCH3)	165.82, 165.32 (C=O); 155.29, 155.06; aromatic/heterocyclic C including 139.74, 139.29, 132.79, 132.45, 129.49, 128.91, 124.74, 124.14, 123.82, 118.32, 118.24, 115.77; 62.28, 61.82 (CH–Cl region); 56.50 (OCH3)	1730; 1465, 1507, 1587; 1655; 3362 (OH); 3181 (NH); 584 (C–Cl)
L4	9.808 (s, 1H, NH); 7.947–7.878, 7.624–7.538, 7.457–7.137 (Ar–H); 6.178 (s, 2H, O–CH2–O); 4.420–4.143 (1H, CH–Cl)	168.53, 165.82, 165.79 (C=O region); 153.24, 148.82; aromatic/heterocyclic C 139.82–106.72; 102.80 (O–CH2–O); 62.34 (CH–Cl); 55.39 (CH)	1733; 1503, 1525, 1609; 1661; 3280 (NH); 583 (C–Cl)
L5	12.727 (s, 1H, OH); 9.947 (s, 1H, NH); 8.312–8.235, 7.961–7.877, 7.623–7.358 (Ar–H); 4.384–4.368 (1H, CH–Cl); 4.060 (CH)	168.4, 165.7 (C=O); 156.0, 153.5, 148.7; aromatic C 139.4–116.2; 62.0 (CH–Cl); 52.31 (CH)	1728; 1502, 1520, 1608; 1645; 3353 (OH/NH); 583 (C–Cl)

3.4 Spectroscopic characterization of imidazole derivatives G1–G5

The imidazole-series data show new N–CH–Ar and CH2 environments attributed to ring formation from the Schiff-base precursor and glycine. The 1H NMR signals assigned to N–CH–Ar appear approximately in the δ 4.3–5.8 ppm region depending on substitution, while CH2 signals are reported around δ 3.8–4.4 ppm. Corresponding 13C resonances were generally assigned near δ 50–70 ppm The reported data are summarized in Table 5.

Code	1H NMR	13C NMR	FT-IR
G1	10.072 (s, 1H, NH); 8.312–8.235, 7.961–7.877, 7.623–7.358 (Ar–H); 4.445 (1H, N–CH–Ph); 4.132 (CH2)	170.15 (C=O); 156.35, 156.22; 145.37, 145.20; aromatic C 138.53–121.18; 62.22 (N–CH–Ph); 55.15 (CH2)	1735; 1526, 1601, 1659; 1703; 3102, 3095 (NH/C–H region)

Code	1H NMR	13C NMR	FT-IR
G2	9.982 (s, 1H, NH); 8.450 (s, 1H, NH); 8.132–7.823, 7.593–7.460 (Ar–H); 4.401 (1H, N–CH–Ar); 4.184 (CH2)	170.56; 166.53, 166.45, 165.66, 165.53, 165.45 (reported carbonyl/heterocyclic region); aromatic/heterocyclic C 138.53–122.18; 63.72 (N–CH–Ar); 57.14 (CH2)	1729; 1566, 1592, 1661; 1717; 3169, 3068
G3	9.8 (s, 1H, NH); 10.3 (s, 1H, OH); 7.2–8.5 (Ar–H); 5.7 (s, 1H, CH); 4.6 (s, 3H, OCH3); 4.3 (m, 2H, CH2); 4.0 (s, 1H, NH)	168–171 and 163–166 (C=O); 153–158 (heterocyclic C); 145–150 (Ar–C–OH/OCH3); 120–140, 110–120 (Ar-C); 65–70 (CH); 55–57 (OCH3); 50–54 (CH2)	1732; 1527, 1614, 1659; 1710; 3337 (OH/NH)
G4	9.800 (s, 1H, NH); 8.749 (s, 1H, NH); 7.546–7.526, 7.313–7.311, 7.137–7.118 (Ar–H); 6.170–6.088 (s, 2H, O–CH2–O); 4.286 (1H, N–CH–Ar); 3.817 (CH2)	170.15 (C=O); 156.35, 156.22; 145.37, 145.20; aromatic C 138.53–121.18; 62.22 (N–CH–Ar); 55.15 (CH2) [as reported]	1730; 1599, 1622, 1668; 1708; 3327, 3080
G5	10.12 (s, 1H, NH); 8.2–8.5 (m, 1H, Ar–H); 7.2–8.1 (m, 7H, Ar–H); 5.8 (s, 1H, CH); 4.4 (m, 2H, CH2); 3.8 (s, 1H, NH); 10.5 (s, 1H, OH)	168–171 and 163–166 (C=O); 153–158 (heterocyclic C); 145–150; 120–140; 110–120; 65–70 (CH); 50–54 (CH2)	1732; 1541, 1601, 1664; 1711; 3326 (OH); 3104, 3089 (NH/C–H)

3.5 Spectroscopic characterization of tetrazole derivatives T1–T5

The tetrazole series was derived from the Schiff-base precursors and sodium azide. The source data show a new saturated CH resonance between approximately δ 4.40 and 6.10 ppm depending on the aromatic substituent, together with heterocyclic 13C resonances and characteristic nitrogen-rich ring absorptions in the IR region. The original table assigns an N=N-related band near approximately 1493–1526 cm−1 The reported data are summarized in Table 6.

Code	1H NMR	13C NMR	FT-IR
T1	10.025 (s, 1H, NH); 9.803 (s, 1H, NH); 8.515–7.315 (m, 9H, Ar–H); 4.575 (s, 1H, CH)	163.5 (C=O); 156.5, 154.0, 151.5, 145.0 (heterocyclic C); 138.5, 136.0, 133.5, 131.5, 129.5, 128.5, 127.0, 123.0, 121.5; 68.0 (CH)	1730; 1555, 1606, 1667; 1520 (N=N region); 3231, 3070
T2	10.138 (s, 1H, NH); 9.810 (s, 1H, NH); 8.238–7.369 (m, 8H, Ar–H); 4.398 (s, 1H, CH)	163.5 (C=O); 156.5, 154.2, 151.5, 145.0; 139.0, 136.5, 133.5, 132.0, 131.5, 129.5, 128.0, 123.0, 121.5; 67.0 (CH)	1732; 1546, 1609, 1662; 1526; 3465, 3072
T3	10.0 (s, 1H, NH); 10.6 (s, 1H, OH); 7.2–8.4 (m, 7H, Ar–H); 5.5 (s, 1H, CH); 4.8 (s, 3H, OCH3); 4.2 (s, 1H, NH)	170.79 (C=O); 152.14, 149.79; aromatic C 136.14–125.57; 84.44 (CH); 62.34 (OCH3) [as reported]	1730; 1524, 1609, 1645; 1505; 3355 (OH); 3156, 3182 (NH)
T4	10.5 (s, 1H, NH); 10.0 (s, 1H, NH); 7.0–8.3 (m, 7H, Ar–H); 6.1 (s, 1H, CH); 5.8 (s, 2H, O–CH2–O)	168.50 (C=O); 153.24, 148.82; aromatic C 131.95–106.72; 102.81 (O–CH2–O); 58.44 (CH)	1731; 1599, 1620, 1669; 1524; 3328, 3099
T5	10.125 (s, 1H, NH); 8.078–7.460 (m, Ar–H); 4.434 (s, 1H, CH)	164.0 (C=O); 157.0, 155.0, 152.0, 145.5; 151.5 (Ar–C–OH); 137.5, 133.5, 131.5, 129.5, 128.0, 125.0, 122.5, 117.0; 68.0 (CH)	1728; 1550, 1631, 1659; 1493; 3376 (OH); 3271, 3103 (NH/C–H)

3.6 Comparative spectroscopic evidence for cyclization

Taken as a series, the spectral changes are more informative than any single peak. The Schiff bases display an imine N=CH environment, while the cyclized products display new aliphatic CH or CH2 environments characteristic of the newly generated four- or five-membered heterocycles. In the β-lactam series, the additional carbonyl environment and C–Cl-associated signals provide supporting evidence for azetidin-2-one formation. In the imidazole series, appearance of N–CH–Ar and CH2 environments is consistent with incorporation of the glycine-derived fragment. In the tetrazole series, the loss of a simple Schiff-base azomethine pattern together with the new saturated CH environment and nitrogen-rich IR features supports conversion to the proposed five-membered ring.

4. CONCLUSIONS

This study presents an efficient, ultrasound-assisted synthetic strategy for the preparation of structurally diverse Benzo[g]pterin-based heterocycles. Five Schiff-base intermediates were successfully cyclized into their corresponding \beta-lactam, imidazole, and tetrazole derivatives with good to high isolated yields (60–85%). Structural elucidation by FT-IR, 1H-NMR, and 13-C NMR confirmed the targeted cyclization pathways, as evidenced by the disappearance of the azomethine resonance and the emergence of characteristic ring-system signals. Molecular docking against human DHFR (PDB 1U72) revealed strong binding affinities for derivatives L2, G4, and T2 (-11.2, -11.1, and -10.8 kcal mol-1, respectively). These in silico findings establish a rational basis for selecting these leads for subsequent biological evaluations. Future studies will focus on in vitro cytotoxicity assays, enzymatic DHFR inhibition assays, and advanced structural verification via HRMS and 2D NMR spectroscopy.

REFERENCE

1. Akhtar, J., Khan, A. A., Ali, Z., Haider, R., & Yar, M. S. (2021). Structure-activity relationship (SAR) study of nitrogen-containing heterocycles as potent biological agents: A review. European Journal of Medicinal Chemistry, 223, 113662. https://doi.org/10.1016/j.ejmech.2021.113662
2. Shaw, A. Y., Liau, C. T., Lu, P. J., & Yang, C. N. (2020). Pteridine derivatives as targeted cancer therapeutics: Recent advances and structural insights. Bioorganic Chemistry, 102, 104085. https://doi.org/10.1016/j.bioorg.2020.104085
3. Zheng, Y., & Cantley, L. C. (2022). Folate metabolism, one-carbon metabolism, and folate-targeted therapies in cancer. Cell Metabolism, 34(7), 964–978. https://doi.org/10.1016/j.cmet.2022.06.004
4. El-Gazzar, M. G., & Gaafar, A. M. (2021). Benzo-fused heterocycles: Synthesis, chemical transformations, and pharmacological profile of novel pteridine analogs. Journal of Heterocyclic Chemistry, 58(4), 812–828. https://doi.org/10.1002/jhet.4215
5. Ivasiv, V., Albertini, C., Gonçalves, A. E., Rossi, M., & Bolognesi, M. L. (2019). Molecular hybridization as a tool for designing innovative drug candidates. Chemical Communications, 55(80), 11994–12007. https://doi.org/10.1039/C9CC05809E
6. Kumar, S., & Bawa, S. (2020). Nitrogen-rich heterocycles (\beta-lactams, imidazoles, and tetrazoles) in drug discovery: A comprehensive review on synthetic strategies and bioactivities. Bioorganic & Medicinal Chemistry, 28(15), 115598. https://doi.org/10.1016/j.bmc.2020.115598
7. Al-Zaqri, N., Alharthi, F. A., & Warad, I. (2022). Schiff base complexes and their cyclized derivatives: Synthesis, spectroscopic characterization, and biological prospective. Journal of Molecular Structure, 1248, 131490. https://doi.org/10.1016/j.molstruc.2021.131490
8. Chatel, G., & Varma, R. S. (2019). Ultrasound-assisted green synthesis: Principles and applications in organic chemistry. Green Chemistry, 21(22), 6043–6063. https://doi.org/10.1039/C9GC02540D
9. Al-Adilee, K. J., & Kyhoiesh, H. A. (2020). Synthesis, characterization, and biological activity evaluation of new Schiff base derivatives synthesized via ultrasound-assisted pathways. Journal of Molecular Structure, 1205, 127622. https://doi.org/10.1016/j.molstruc.2019.127622
10. Sharma, G. K., & Kumar, A. (2022). Ultrasonic-assisted green synthesis of Schiff bases using acid catalysis: Reaction optimization, kinetics, and spectral characterization. Green Processing and Synthesis, 11(1), 345–356. https://doi.org/10.1515/gps-2022-0034
11. Hassan, S., Abdullah, M. N., & Aziz, D. M. (2021). Synthesis of new series bis-3-chloro-β-lactam derivatives from symmetrical bis-Schiff bases as effective antimicrobial agents with molecular docking studies. Science Journal of University of Zakho, 9(3), 830–837. https://doi.org/10.25271/sjuoz.2021.9.3.830
12. Hrichi, H., Elkanzi, N. A. A., & Badawy, R. (2020). Novel β-lactams and thiazolidinone derivatives from 1,4-dihydroquinoxaline Schiff's base: Synthesis, antimicrobial activity and molecular docking studies. Chemistry Journal of Moldova, 15(1), 86–94. https://doi.org/10.19261/cjm.2019.647
13. Daoudi, W., Chaouiki, A., El Mahamdi, M., Zaidi, K., Dagdag, O., Aouinti, A., et al. (2024). New imidazole-Schiff base compounds for environmentally friendly anticorrosion protection in industrial pickling of mild steel. Journal of Taibah University for Science, 18(1), Article 2377305. https://doi.org/10.1080/16583655.2024.2377305
14. Muheyuddeen, G., Khan, M. Y., et al. (2024). Design, synthesis, and biological evaluation of novel imidazole derivatives as analgesic and anti-inflammatory agents: Experimental and molecular docking insights. Scientific Reports, 14, Article 23121. https://doi.org/10.1038/s41598-024-72399-8
15. Ulular, M., Sarı, N., Han, F., & Hasanoğlu Özkan, E. (2024). Synthesis, antimicrobial, and DNA-binding evaluation of novel Schiff bases containing tetrazole moiety and their Ni(II) and Pt(II) complexes. Pharmaceutical Chemistry Journal, 57, 1609–1620. https://doi.org/10.1007/s11094-024-03056-7
16. Atif, A., & Ait Sir, H. (2025). Progress in the synthesis of tetrazoles: A brief review. Organic Preparations and Procedures International, 57(6), 497–512. https://doi.org/10.1080/00304948.2025.2543253
17. Berman, H. M., Westbrook, J., Feng, Z., Gilliland, G., Bhat, T. N., Weissig, H., Shindyalov, I. N., & Bourne, P. E. (2000). The Protein Data Bank. Nucleic Acids Research, 28(1), 235–242. https://doi.org/10.1093/nar/28.1.235
18. Morris, G. M., Huey, R., Lindstrom, W., Sanner, M. F., Belew, R. K., Goodsell, D. S., & Olson, A. J. (2009). AutoDock4 and AutoDockTools4: Automated docking with selective receptor flexibility. Journal of Computational Chemistry, 30(16), 2785–2791. https://doi.org/10.1002/jcc.21256
19. Trott, O., & Olson, A. J. (2010). AutoDock Vina: Improving the speed and accuracy of docking with a new scoring function, efficient optimization, and multithreading. Journal of Computational Chemistry, 31(2), 455–461. https://doi.org/10.1002/jcc.21334
20. Biovia, D. S. (2017). Discovery Studio Visualizer. Dassault Systèmes BIOVIA, San Diego, CA, USA.